13th ewtec 2019 Proceedings of the 13th European Wave and Tidal Energy Conference 1-6 Sept 2019, Naples, Italy

Submerged pressure differential plate wave energy converter with variable geometry

Nathan Tom, Yi-Hsiang Yu, and Alan Wright

Abstract—**This work presents a novel wave energy converter device concept that combines a submerged pressure differential plate with variable geometry modules. The two variable geometry sections, placed at the fore and aft locations on the plate, consist of five identical flaps that are opened in ascending order starting with the flaps closest to the edges of the plate and moving inward. The variable geometry modules act as control surfaces that allow for the hull geometry to be adjusted, leading to changes in the hydrodynamics. The device geometry is controlled in a quasi-static fashion while the power take-off (PTO) unit would be controlled on a wave-to-wave timescale. The submerged plate is tethered directly to the seabed by integrated mooring and PTO lines, eliminating the need for a second reaction body. A linear frequency domain analysis is used to evaluate device performance in terms of absorbed power, PTO force, and absorber body motion. The frequency domain analysis required the linearization of the PTO dynamics to couple the fore and aft PTOs to the motion of the absorber body. The inclusion of the variable geometry modules was shown to be effective at altering the device geometry to provide changes in the absorber hydrodynamics to produce measurable reductions in structural and PTO loading.**

Index Terms—**Hydrodynamics, Load Reduction, Submerged Wave Energy Converter, Variable Geometry**

I. Introduction

At the 11th and 12th European Wave and Tidal Energy Conference (EWTEC), a fixed-bottom oscillating surge wave energy converter (OSWEC) [1] was introduced that replaced the main body with control surfaces [2], [3]. The intent of the control surfaces was to allow for the wave energy converter (WEC) to change the hull geometry such that the hydrodynamic characteristics will favor either power absorption or load shedding. This variable geometry concept arose from a structued innovation approach to the development of WECs in hopes of achieving a step reduction in the high cost of energy for marine energy devices [4]. While, the application of large-scale geometric variability in WECs has been considered in the design of the WEPTOS [5], a surface floating and slack-moored structure, composed of two symmetrical legs, each supporting a large number of identical rotors, connected by a crossbeam to form an A-frame. The crossbeam can be moved forward and backward, allowing for shape adaptability, which will increase its width relative to the incoming wave power in regular operating conditions and reduce its width and interaction with excessive wave power in larger and extreme wave conditions. Another WEC under development that considers controlling power absorption by varying the converter position in the water column is Marine Power Systems's (MPS') WaveSub [6]. The WaveSub consists of a small power-capturing float and a bottom high-inertia reaction barge with the float connected to the power take-off (PTO) system contained on the reaction barge. The relative positioning of the float and reaction barge is made possible by operating winches that change the mooring line length and the tether line length between the float and barge. However, like the WEPTOS, the hydraulic winches have been designed to adjust the tether lines and mooring length on a sea-state-by-sea-state basis, while the variable geometry modules proposed in [7] would be controlled on a wave-to-wave timescale.

The variable geometry OSWEC concept was shown in papers and wave tank studies to be successful at mitigating loads in moderate-to-large sea states [8], [9]. It combines manipulation of the variable geometry components with PTO control in an attempt to control peak loads rather than focus on power maximization [10], [11]. However, the bottom-fixed OSWEC is limited in the number of deployment sites and the response is restricted to one degree of freedom. We wanted to explore the influence of variable geometry modules on the hydrodynamics of a WEC oscillating in three degrees of freedom and that could also be deployed in deeper water. In response, a submerged pressure differential plate WEC that was tethered at each of its four corners to the seabed was chosen for this work. This WEC design allows for surge, heave, and pitch motion, which, depending on the orientation of the PTO to the tethers, can all contribute to power absorption.

Previous investigations into submerged WEC devices date back to the first publications on the Bristol Cylinder [13], which comprises a submerged long circular cylinder in motion beneath the waves and is constrained by a system of vertical and horizontal springs and dampers. The advantages of the Bristol

The paper was given ID number 1699 and was submitted to the wave device development and testing thematic track. The Alliance for Sustainable Energy, LLC (Alliance) is the manager and operator of the National Renewable Energy Laboratory (NREL). NREL is a national laboratory of the U.S. Department of Energy, Office of Energy Efficiency and Renewable Energy. This work was authored by the Alliance and supported by the U. S. Department of Energy under Contract No. DE-AC36-08GO28308. Funding was provided by the U.S. Department of Energy Wind Energy Technologies Office. The views expressed in the article do not necessarily represent the views of the U.S. Department of Energy or the U.S. government. The U.S. government retains, and the publisher, by accepting the article for publication, acknowledges that the U.S. government retains a nonexclusive, paid-up, irrevocable, worldwide license to publish or reproduce the published form of this work, or allow others to do so, for U.S. government purposes.

N. Tom, Y.H. Yu and A. Wright are with the National Renewable Energy Laboratory 15013 Denver West Parkway, Golden, CO 80401 U.S.A (e-mail: nathan.tom@nrel.gov).

Cylinder are that operation is just below the ocean surface, shedding excessive power levels and oscillating in such a way as to reduce excessive wave loading and avoid end stop problems [14]. These operating principles are present in CalWave Power Technologies' WEC design, which was inspired by a flexible underwater carpet [15]. A revised deep water WEC design helped CalWave Power Technologies take second place in the U.S. Department of Energy Wave Energy Prize [16] in 2016. In addition to [13], a submerged sphere with a single and a three-cable integrated mooring and PTO system was investigated in [17] that demonstrated similar power absorption characteristics to a floating sphere. These results appear to have helped guide Carnegie Clean Energy's decision to move from a single moored configuration in the CETO 6 generation technology to a multimoored configuration that can theoretically absorb up to three times more power than heave motion alone [18].

This paper begins with a physical description of the base design and operation of the proposed pressure differential plate WEC, device mass properties, and the additional hydrostatic force required to keep the main absorber body submerged. The paper then linearizes the dynamics of the combined PTO and mooring tethers to construct a linear system dynamics model that includes the three degree-of-freedom absorber body. The analysis will be completed in the frequency domain under regular wave excitation with a constraint set on the PTO displacement to prevent any part of the device from breaching the sea surface. After setting up the linear system dynamic model, the paper introduces the location, size, and proposed operation of the variable geometry modules. The change in the surge, heave, and pitch hydrodynamics with manipulation of the variable geometry modules is first discussed to provide insight into the effect on power absorption, PTO forces, and absorber body motion.

II. Device Description

The base device considered in this study can be modeled as a submerged rectangular plate with length (along the x-axis), l; width (along the y-axis), w; and thickness (along the z-axis), t, that has a center of gravity submerged at a depth, d, beneath the calm water surface; refer to Fig. 1. The plate will be connected directly to the seabed with four vertical tethers in a water depth, h. The tethers will be attached at the four corners of the rectangular plate where a ball and socket joint acts as the connection between the plate-tether and the seabed-tether intersections. Each tether will not be allowed to bend, but can rotate as well as extend and compress in the axial direction to satisfy the kinematic constraints. The kinetic and potential energy of the rectangular plate, driven by the incident waves, will be absorbed by the tethers that act as PTO systems and will be modeled as separate spring-damper systems.

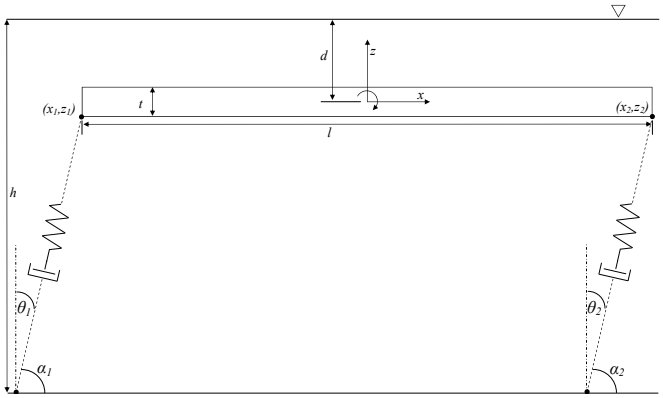

Fig. 1. Coordinate system for the device under investigation.

A. Mass Properties

A submerged rectangular plate, with a uniform mass distribution, will have the following inertial properties:

$$m = \rho_m l w t \tag{1}$$

$$m_d = \rho l w t \tag{2}$$

$$f_h = \left(1 - \frac{\rho_m}{\rho}\right) \rho g l w t = (1 - m_f)\, \rho g l w t \tag{3}$$

$$I_{55} = \frac{m l^2}{12}\left(1 + \left(\frac{t}{l}\right)^2\right) \tag{4}$$

where m is the mass of the plate, m_d is the fluid displaced mass, f_h is the hydrostatic force arising from the difference between the WEC weight and buoyancy forces, and I_{55} is the pitch mass moment of inertia around the plate center of gravity. The variable ρ_m is the material mass density; ρ is the fluid density; m_f is the mass fraction, which is equal to the ratio of the material-to-fluid mass densities, and g is the gravitational acceleration.

The plate will be designed to have positive buoyancy, which requires the material mass density to be less than the fluid density ($\rho_m < \rho$). The hydrostatic force of the plate must be matched to prevent the body from rising to the surface. This is possible by selecting the correct spring stiffness used in the tether PTO model. The spring coefficient for each PTO, attached at each corner of the plate, will be constant and calculated from the hydrostatic force and the initial spring extension length:

$$C_g = \frac{f_h}{n l_s} = \frac{(1 - m_f)\, \rho g l w t}{n l_s} \tag{5}$$

where n is the number of PTO units and l_s is the spring extension length in calm water; we assumed that the spring has no initial pretension. The total heave restoring coefficient is then given by $C_{33} = f_h / l_s$. The linearized pitch restoring torque for the PTO located at $(x = -l/2,\ y = -w/2)$ is given by the following formula:

$$\begin{aligned} \tau_{g1} &= -\frac{l}{2}\left(C_g \frac{l}{2} \sin\zeta_5\right) = -C_g \left(\frac{l}{2}\right)^2 \sin\zeta_5 \\ &\approx -C_g \left(\frac{l}{2}\right)^2 \zeta_5 \ ,\ \zeta_5 << 1 \end{aligned} \tag{6}$$

where the small angle approximation has been made to obtain the final form of the equation.

In this work, only plane progressive waves will be considered, which prevents sway, roll, and yaw motion. The analysis can then be simplified to only two tether PTO units located at either end of the plate. The total linearized pitch restoring coefficient is given by the following equation:

$$C_{55} = \frac{f_h}{l_s}\left(\frac{l}{2}\right)^2 \tag{7}$$

III. POWER TAKE-OFF DYNAMIC MODELING

The connection points between the fore and aft PTO units with the plate are denoted by the coordinates x_1, z_1 and x_2, z_2, respectively, and are shown in Fig. 1. The position time history of the fore and aft connection points are given by the following equations:

$$x_1(t) = \zeta_1(t) - \frac{l}{2}\cos\zeta_5(t) \tag{8}$$

$$z_1(t) = \zeta_3(t) + \frac{l}{2}\sin\zeta_5(t) + (h-d) \tag{9}$$

$$x_2(t) = \zeta_1(t) + \frac{l}{2}\cos\zeta_5(t) \tag{10}$$

$$z_2(t) = \zeta_3(t) - \frac{l}{2}\sin\zeta_5(t) + (h-d) \tag{11}$$

where ζ_1 is the time-varying surge motion of the plate, ζ_3 is the time-varying heave motion of the plate, and ζ_5 is the time-varying pitch motion of the plate. The angle at which the tether PTO rotates from vertical, θ, can be calculated from the following:

$$\tan\theta_1 = \frac{x_1 + \frac{l}{2}}{z_1} = \frac{\zeta_1 + \frac{l}{2}(1-\cos\zeta_5)}{\zeta_3 + \frac{l}{2}\sin\zeta_5 + h - d} \tag{12}$$

$$\tan\theta_2 = \frac{x_2 - \frac{l}{2}}{z_2} = \frac{\zeta_1 - \frac{l}{2}(1-\cos\zeta_5)}{\zeta_3 - \frac{l}{2}\sin\zeta_5 + h - d} \tag{13}$$

As seen from the above expressions, the tether PTO dynamics consist of coupled nonlinear equations that can be solved as an initial value problem. However, it is of interest to construct a linear model to describe the tether PTO dynamics for initial design iterations. It is possible to start linearizing the PTO dynamics by making the small angle approximation, $\zeta_5 << 1$. The small angle approximation will allow the PTO rotation angles to be simplifed to the following equations:

$$\tan\theta_1 = \frac{\frac{\zeta_1}{h-d}}{\frac{\zeta_3}{h-d} + \frac{l}{2(h-d)}\zeta_5 + 1} \tag{14}$$

$$\tan\theta_2 = \frac{\frac{\zeta_1}{h-d}}{\frac{\zeta_3}{h-d} - \frac{l}{2(h-d)}\zeta_5 + 1} \tag{15}$$

The tether PTO stroke length will then be simplified to the following equations:

$$\frac{\Delta L_1}{h-d} \approx \sqrt{\left(\frac{\zeta_1}{h-d}\right)^2 + \left(\frac{\zeta_3}{h-d} + \frac{l}{2}\frac{\zeta_5}{h-d} + 1\right)^2} - 1 \tag{16}$$

$$\frac{\Delta L_2}{h-d} \approx \sqrt{\left(\frac{\zeta_1}{h-d}\right)^2 + \left(\frac{\zeta_3}{h-d} - \frac{l}{2}\frac{\zeta_5}{h-d} + 1\right)^2} - 1 \tag{17}$$

where ΔL_1 and ΔL_2 are the PTO displacements, from static equilibirum, of the fore and aft PTO units. The PTO stroke velocity can now be simplified to:

$$\Delta\dot{L}_1 \approx \frac{\left(\dot{\zeta}_1 + \frac{l}{2}\dot{\zeta}_5\zeta_5\right)\zeta_1 + \left(\dot{\zeta}_3 + \frac{l}{2}\dot{\zeta}_5\right)\left(\zeta_3 + \frac{l}{2}\zeta_5 + (h-d)\right)}{\sqrt{(\zeta_1)^2 + \left(\zeta_3 + \frac{l}{2}\zeta_5 + (h-d)\right)^2}} \tag{18}$$

$$\Delta\dot{L}_2 \approx \frac{\left(\dot{\zeta}_1 - \frac{l}{2}\dot{\zeta}_5\zeta_5\right)\zeta_1 + \left(\dot{\zeta}_3 - \frac{l}{2}\dot{\zeta}_5\right)\left(\zeta_3 - \frac{l}{2}\zeta_5 + (h-d)\right)}{\sqrt{(\zeta_1)^2 + \left(\zeta_3 - \frac{l}{2}\zeta_5 + (h-d)\right)^2}} \tag{19}$$

To further simplify the expressions, the following approximation will be made:

$$\frac{\zeta_1}{h-d} << \frac{\zeta_3}{h-d} \pm \frac{l}{2}\frac{\zeta_5}{h-d} + 1 \tag{20}$$

which states that the surge displacement is much smaller than the vertical position of the PTO connection point to the absorber body. This claim is strengthened as the quantity, $h-d$, becomes larger because the surge displacement must be even larger before it has a significant effect on the PTO elongation. However, a condition that bounds the accuracy of this approximation should be derived and it will be assumed that up to a 5% error is allowable for the small angle approximations. With this accuracy requirement,the maximum rotational angles to stay within the small angle approximation can be calculated from the Taylor series expansion of the cosine and sine functions as follows:

$$\sin\theta \approx \theta - \frac{\theta^3}{3!} + \left(O^5\right) + \ldots = 0.95\theta \rightarrow \theta_{ls} = 0.548 \tag{21}$$

$$\cos\theta \approx 1 - \frac{\theta^2}{2!} + \left(O^4\right) + \ldots = 0.95 \rightarrow \theta_{lc} = 0.316 \tag{22}$$

where θ_{ls} and θ_{lc} are the maximum rotation angles allowed before exceeding the 5% error in the small angle approximations for sine and cosine. The smallest allowable rotation is obtained when meeting the small angle approximation for the cosine function. This limiting rotation can be used to estimate the maximum horizontal displacement allowed before the small angle assumption may need to be readdressed:

$$\tan\theta_{lc} \approx \frac{\zeta_1}{h-d} \rightarrow \zeta_1 \approx \frac{1}{3}(h-d) \tag{23}$$

where the time-averaged vertical position has been used for the height. Therefore, if the surge displacement does not exceed one-third of the mean vertical position of the plate, then the sine and cosine small angle approximations should remain valid.

The approximation given by (20) allows for further simplification of the PTO stroke length:

$$\Delta L_1 \approx \zeta_3 + \frac{l}{2}\zeta_5 \tag{24}$$

$$\Delta L_2 \approx \zeta_3 - \frac{l}{2}\zeta_5 \tag{25}$$

For the PTO stroke velocity, further simplification is needed before a linearized model can be obtained. This can be achieved by neglecting any second or higher order terms resulting in the following linearized equations:

$$\Delta\dot{L}_1 \approx \frac{\left(\dot{\zeta}_1 + \frac{l}{2}\dot{\zeta}_5\zeta_5\right)\zeta_1 + \left(\dot{\zeta}_3 + \frac{l}{2}\dot{\zeta}_5\right)\left(\zeta_3 + \frac{l}{2}\zeta_5 + (h-d)\right)}{\zeta_3 + \frac{l}{2}\zeta_5 + (h-d)}$$
$$\approx \dot{\zeta}_3 + \frac{l}{2}\dot{\zeta}_5 \tag{26}$$
$$\Delta\dot{L}_2 \approx \frac{\left(\dot{\zeta}_1 - \frac{l}{2}\dot{\zeta}_5\zeta_5\right)\zeta_1 + \left(\dot{\zeta}_3 - \frac{l}{2}\dot{\zeta}_5\right)\left(\zeta_3 - \frac{l}{2}\zeta_5 + (h-d)\right)}{\zeta_3 - \frac{l}{2}\zeta_5 + (h-d)}$$
$$\approx \dot{\zeta}_3 - \frac{l}{2}\dot{\zeta}_5 \tag{27}$$

The linearized axial force generated along the fore and aft PTO tethers will take the form of:

$$f_{m1} = -C_g\Delta L_1 - \lambda_g\Delta\dot{L}_1 \tag{28}$$
$$f_{m2} = -C_g\Delta L_2 - \lambda_g\Delta\dot{L}_2 \tag{29}$$

where λ_g is the PTO linear-damping coefficient and it has been assumed each PTO unit has the same damping value. Future work will consider optimizing power absorption using different PTO damping coefficients for each PTO unit. The force from each PTO has been developed in radial coordinates; however, because of the PTO rotation around the vertical axis, the PTO force must be converted into Cartesian coordinates. The derivation of the linearized horizontal and vertical components of the PTO force was completed during this work; however, the length of the derivation is prohibitive to stay within the page limit for this conference. The full derivation and supporting approximations will be published in a follow-on article.

IV. Regular Wave Analysis

Under regular wave excitation, the surface profile of a right propagating incident wave can be described by the following equation:

$$\eta(x,t) = \Re\left\{Ae^{i(\omega t - kx)}\right\} = A\cos(\omega t - kx) \tag{30}$$

where η is the wave elevation, A is the wave amplitude, ω is the wave angular frequency, k is the wave number, $i = \sqrt{-1}$ is the imaginary unit, and $\Re$ is the real component of the argument. The plate will oscillate in the surge, heave, and pitch modes which can be described by the following linear coupled system of equations:

$$\begin{bmatrix} AX_1 \\ AX_3 \\ AX_5 \end{bmatrix} = M \begin{bmatrix} i\omega\xi_1 \\ i\omega\xi_3 \\ i\omega\xi_5 \end{bmatrix} \tag{31}$$

$$\begin{aligned}
M(1,1) &= \lambda_{11} + i\left[\omega(m+\mu_{11}) - \frac{f_h}{\omega(h-d)}\right] \qquad (32)\\
M(1,3) &= \lambda_{15} + i\omega\mu_{15}\\
M(2,2) &= \lambda_{33} + 2\lambda_g + i\left[\omega(m+\mu_{33}) - C_{33}/\omega\right]\\
M(3,1) &= \lambda_{51} + i\omega\mu_{51} = \lambda_{15} + i\omega\mu_{15}\\
M(3,3) &= \lambda_{55} + 2\lambda_g\left(\frac{l}{2}\right)^2 + i\left[\omega(I_{55}+\mu_{55}) - C_{55}/\omega\right]
\end{aligned}$$

where ξ_j is the complex displacement amplitude for oscillation mode j; X_j is the complex wave exciting force or torque, per unit wave amplitude, for oscillation mode j; μ_{jk} is the radiation added mass (or added moment of inertia) in oscillation mode j due to oscillation mode k; and λ_{jk} is the radiation wave damping in oscillation mode j due to oscillation mode k. Equation (31) shows that for the three modes of motion used to absorb the incident wave power, only the surge-pitch equations of motion are coupled. The decoupled motion between heave and surge-pitch is a consequence of the linear hydrodynamics and the small amplitude assumptions made to linearize the equations of motion.

The mechanical force from each PTO unit is described by the following equations:

$$\begin{aligned}
\frac{\alpha_{m1}}{A} &= \left[\lambda_g - iC_g/\omega\right] i\omega\frac{\xi_3 + \frac{l}{2}\xi_5}{A} \qquad (33)\\
&= \left[\lambda_g - iC_g/\omega\right] i\omega\frac{\Lambda_1}{A}\\
\frac{\alpha_{m2}}{A} &= \left[\lambda_g - iC_g/\omega\right] i\omega\frac{\xi_3 - \frac{l}{2}\xi_5}{A} \qquad (34)\\
&= \left[\lambda_g - iC_g/\omega\right] i\omega\frac{\Lambda_2}{A}
\end{aligned}$$

where α_{m1} and α_{m2} represent the complex PTO force amplitudes for PTO 1 and PTO 2, respectively, while Λ_1 and Λ_2 represent the complex PTO displacement amplitudes for PTO 1 and PTO 2. The time-averaged power absorbed by each PTO unit can be modeled by the following equations:

$$\frac{P_{T1}}{A^2} = \frac{\lambda_g\omega^2}{2}\left|\frac{\xi_3 + \frac{l}{2}\xi_5}{A}\right|^2 \tag{35}$$
$$\frac{P_{T2}}{A^2} = \frac{\lambda_g\omega^2}{2}\left|\frac{\xi_3 - \frac{l}{2}\xi_5}{A}\right|^2 \tag{36}$$

where P_{T1} and P_{T2} represent the time-averaged power for PTO 1 and PTO 2, respectively. In this case, the spring constant represents a mechanical spring and thus the spring energy is assumed to be conservative with no bidirectional energy flow.

The power absorbed by each PTO unit will be near equal when the pitch motion is minimized, which can be expected for longer wave lengths. However, as wave length decreases, the contribution to the total power capture from each PTO unit becomes less uniform and will be dependent on the phase difference between absorber body heave and pitch motion.

To provide a measure of efficiency, the time-averaged power contained within a propagating wave must be known. The time-averaged wave-power-per-unit width, P_w, can be calculated as follows:

$$P_w = \frac{1}{4}\rho g A^2\sqrt{\frac{g}{k}\tanh kh}\left[1 + \frac{2kh}{\sinh 2kh}\right] \tag{37}$$

where h is the water depth. The nondimensional capture width, C_w, will be defined as:

$$C_w = \frac{P_T}{w_e P_w} = \frac{P_{T1} + P_{T2}}{w_e P_w} \tag{38}$$

TABLE I
GEOMETRIC PARAMETERS FOR VARIABLE GEOMETRY SUBMERGED PLATE HYDRODYNAMIC MODELING.

Dimension	Variable	Unit
Water Depth	h	10.00 m
Submerged Depth	d	1.40 m
Thickness	t	0.80 m
Width	w	10.00 m
Length	l	20 m
Volume	$\forall$	137.5 m^3
Flap Section Width	f_w	9.00 m
Flap Section Length	f_l	2.50 m
Flap Separation Width	f_s	14.00 m
Flap Side Width	w_s	0.50 m
Flap Width	f_d	0.50 m
Flap Thickness	t_f	0.30 m
Displaced Mass	m	45.25 t
Moment of Inertia	I_{55}	2.46 kt·m^2

$$w_e = w\sqrt{1+\left(\frac{l}{w}\right)^2} \tag{39}$$

where P_T is the sum of the absorbed power by both PTO units and w_e is the equivalent width of the plate. One might chose to nondimensionalize using the width of the plate perpendicular to the wave front; however, this will not take into account the length of the plate, which could be several times greater than the width [19]. In this case, the capture width may be overinflated and the equivalent width may do a better job of representing the capital costs associated with constructing a longer absorber body.

V. VARIABLE GEOMETRY SUBMERGED PLATE

The variable geometry absorber body is shown in Fig. 2. The length of the plate, l, was set at 20 m; the plate width, w, was set at 10 m; the plate thickness, t, was set at 0.8 m; the submergence depth, d, was set at 1.4 m; and the water depth, h, was fixed at 10 m. The primary dimensions were chosen so results could be compared against the load and power performance of a bottom-fixed oscillating surge WEC with the same primary dimensions as described in [7]. The variable geometry modules have been placed along the x-axis at the front and back of the absorber body. The geometric dimensions of the variable geometry modules have been listed in Table I.

The fore and aft variable geometry modules consist of five identical flaps. The flaps were allowed to rotate around their central axis, which corresponds to the geometric center, and will be measured by the angle φ; see Fig. 3. The flaps have a thickness, t_f, of 0.3 m; a length, f_d, of 0.5 m; and rounded edges with a radius of 0.15 m. The variable geometry enabling flaps are controlled in a binary fashion, in which the actuators inside the WEC allow for only fully closed, $\varphi = 0$ deg, or fully open, $\varphi = 90$ deg, configurations. In the closed configuration, a flap will lie parallel to the length of the main absorber body. When all flaps are in the closed configuration, there will be no openings in the WEC geometry and the wave pressure will be maximized on the top surface of the absorber body. In the open configuration, a flap will be oriented perpendicular to the length of the main absorber body. When all flaps are in the open configuration, there will be openings in the WEC geometry and the wave pressure will be minimized on the top surface of the absorber body. The flaps may be opened independently, but will only be allowed to open in ascending order starting with the flap located closest to the sides of the absorber body and moving inward. Therefore, no geometry is modeled that consists of a closed flap between two open flaps.

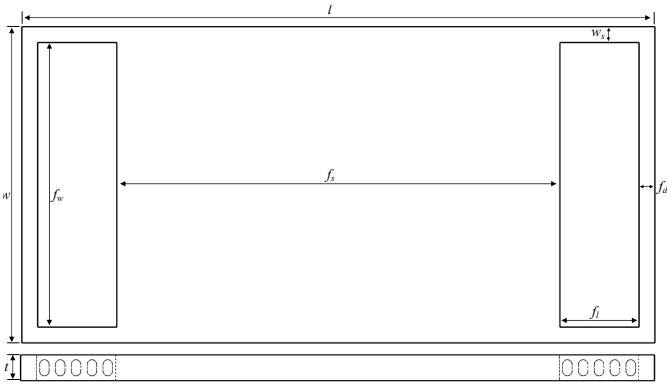

Fig. 2. Top and side view of the variable geometry heave plate wave energy converter. In the side view, all variable geometry module flaps have been rotated to the open configuration ($\varphi = 90^o$).

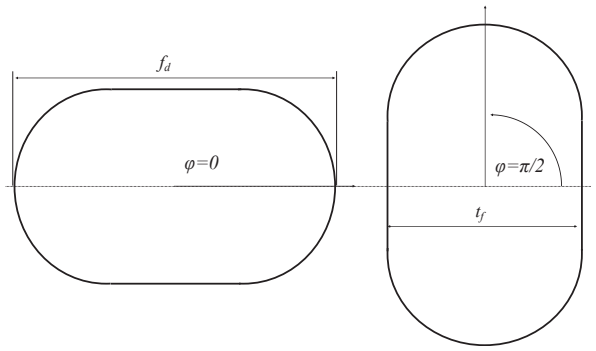

Fig. 3. (Left) Side view of a single variable geometry flap in the closed configuration, $\varphi = 0$ deg, and (Right) Side view of a single variable geometry flap in the open configuration, $\varphi = 90$ deg.

A. Variable Geometry Submerged Plate Hydrodynamics

The surge, heave, and pitch hydrodynamic coefficients were calculated using WAMIT version 7.2 [20] and must be obtained before the power and load performance of the WEC can be estimated. The hydrodynamic radiation and excitation coefficients, obtained from WAMIT, are nondimensionalized and plotted in Fig. 4 while varying the number of flaps that were opened. The surge, heave, and pitch hydrodynamic coefficients were obtained with a submergence depth of 1.4 m to provide 1 m of water above the plate. Because the mass density has been assumed uniform, the center of gravity sits 0.4 m below the top of the plate and the depth of submergence has been defined as the vertical distance from the still water line to the plate center of gravity. The device has been designed to

remain immersed, and a shallower submergence depth will limit the heave and pitch motion amplitudes, leading to a reduction in maximum power capture [21]. For nondimensionalization, a mass fraction of one-third has been chosen for calculating the plate mass and moment of inertia.

Beginning with the surge hydrodynamics, the added mass and wave damping radiation coefficients, Fig. 4a, are indeed influenced by the opening of the variable geometry flaps. The surge added mass is the only radiation coefficient that increases as each additional flap is opened. This phenomena is likely attributed to the additional fluid sitting between adjacent open flaps that must now be accelerated when the absorber body surges. The surge radiation wave damping peak value decreases and shifts to higher wave angular frequencies as each additional flap is opened. The reduction between 0 and 5 open flaps is slightly less than 40%, which exceeds the ratio of the absorber body plane form, which is only reduced by approximately 10%. In Fig. 4b, the peak surge-wave excitation force has also been observed to move to higher frequencies with a decreasing peak magnitude as each additional flap is opened.

The heave hydrodynamic coefficients are the least sensitive when actuating the variable geometry flaps but are still reduced in magnitude. However, an interesting result for the heave added mass occurs in the nondimensional wave angular frequency range of 0.9 to 1.3, where negative added mass values are present; see Fig. 4c. This phenomenon has been observed for submerged bodies when the depth of submergence is sufficiently small compared to the thickness of the oscillating body [22]. The negative added mass values are generally associated with standing waves that are generated around the floating body or antisymmetric sloshing modes for water trapped between multiple hulls with close spacing [23]. Although the calculation of the added mass can be negative for specific frequency ranges, the diagonal radiation wave damping coefficients must be nonnegative, as they are measures of the energy flux in the waves radiating away from the oscillating body [24]. The heave-wave excitation force decreases at approximately the same rate as the reduction in the plane form area of the absorber body; see Fig. 4d. Unlike a surface piercing body, where the heave wave-excitation force converges to the heave restoring coefficient in long waves, for a submerged device, the heave wave-excitation force will tend to 0 in long waves. The authors believe that the heave hydrodynamic coefficients are less sensitive to the openings controlled by the variable geometry flaps because the hydrodynamic pressure generated by the diffracted wave and device motion are concentrated at the center of the plate rather than on the sides [7].

The pitch hydrodynamic coefficients are the most sensitive to the opening of the variable geometry flaps. For the radiation coefficients, this means the fluid surrounding the pitching plate has an easier time wrapping around the plate edges, reducing the vertical added mass near the plate ends. The vertical added mass can be related to the pitch added moment of inertia by the square of the distance from the center of gravity to the point of application. It is expected that the frequency for resonant pitch motion will shift across a wider frequency range compared to the surge and heave motions. Thus, the pitch radiation coefficient peaks are reduced by approximately 65% (see Fig. 4e) while the peak pitch wave-exciting torque is reduced by approximately 50% (see Fig. 4f). Furthermore, the surge-pitch radiation coefficients appear to have almost a binary response between the 0 and 1 flap open configurations. As seen from Fig. 5, unlike the gradual reduction in the surge, heave, and pitch radiation coefficients when opening the flaps, the surge-pitch radiation coefficients have a large reduction when the first flap is opened with little variation as additional flaps are opened.

B. Variable Geometry Submerged Plate Regular Wave Results

With the hydrodynamic coefficients obtained from WAMIT, the surge, heave, and pitch motion of the plate can be calculated from (31) after selecting the PTO spring and damping coefficients. The plate motion and PTO coefficients are used to calculate the absorbed power and axial force for PTO 1 and PTO 2 from (33)-(36). In an effort to maximize the total power capture, the spring extension length, l_s, was selected to be 1 m (which determines the heave and pitch restoring coefficients), and the mass fraction, m_f, was selected to be one-third, while varying the linear PTO damping coefficient until a maximum in power capture was found. For this analysis, the linear PTO damping coefficient is constant for each PTO; however, it may be possible to further optimize power production with different damping coefficients for each PTO unit. The analysis also placed a constraint on the system to ensure the motion of the plate did not pass above the still water line. Therefore, when calculating the maximum power capture, the following motion limit was not to be exceeded:

$$\left|\frac{\Delta L_1}{A}\right| = \left|\frac{\xi_3 + \frac{l}{2}\xi_5}{A}\right| < d - t/2 \tag{40}$$

$$\left|\frac{\Delta L_2}{A}\right| = \left|\frac{\xi_3 - \frac{l}{2}\xi_5}{A}\right| < d - t/2 \tag{41}$$

These expressions limit the response amplitude operator of the axial stroke to less than or equal to $d - t/2$ up to a wave amplitude of 1 m. Once the wave amplitude increases past 1 m, it is expected that nonlinear wave effects will have greater importance and the linear model proposed in this work may not provide sufficient accuracy to evaluate the WEC performance.

The maximum absorbed power for the fore and aft PTO units for each variable geometry flap configuration has been plotted in Fig. 6a. In Fig. 6a, the PTO units have different power outputs, with the aft PTO providing more than 90% of the energy capture for a range of wave frequencies; see Fig. 7. For each flap configuration, there are wave frequencies at which PTO 1 produces almost no power, which can be attributed

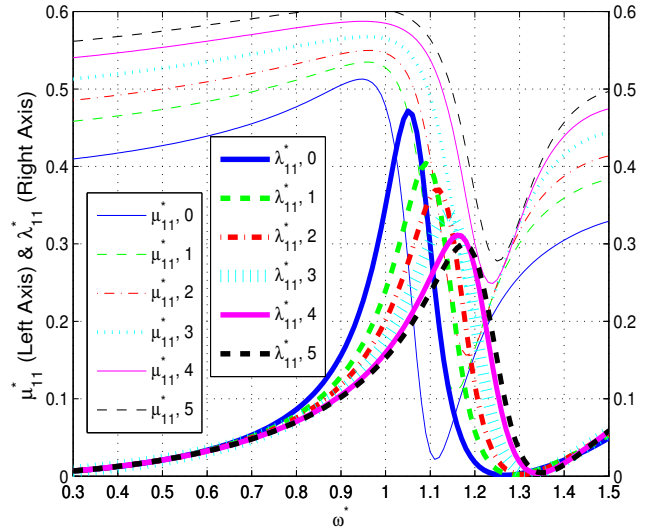

(a) Surge-wave damping λ_{11} and added mass μ_{11}

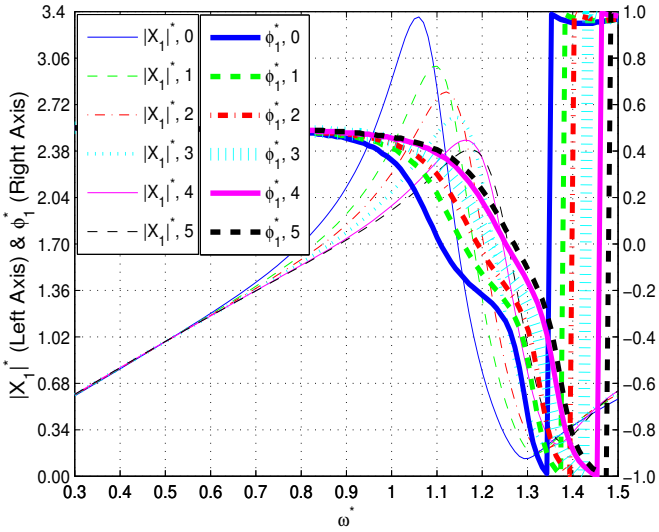

(b) Surge-wave exciting torque magnitude $|X_1|$ and phase ϕ_1

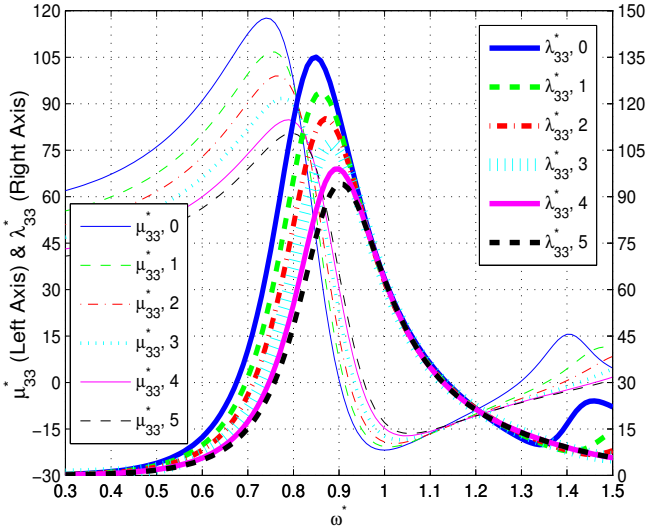

(c) Heave-wave damping λ_{33} and added mass μ_{33}

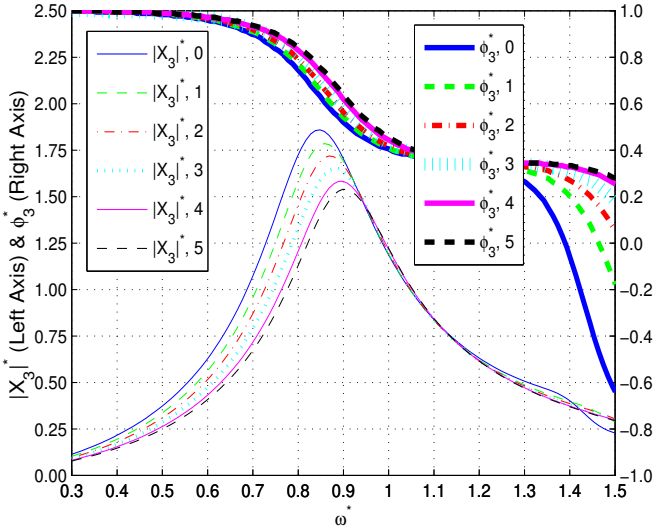

(d) Heave-wave exciting force magnitude $|X_3|$ and phase ϕ_3

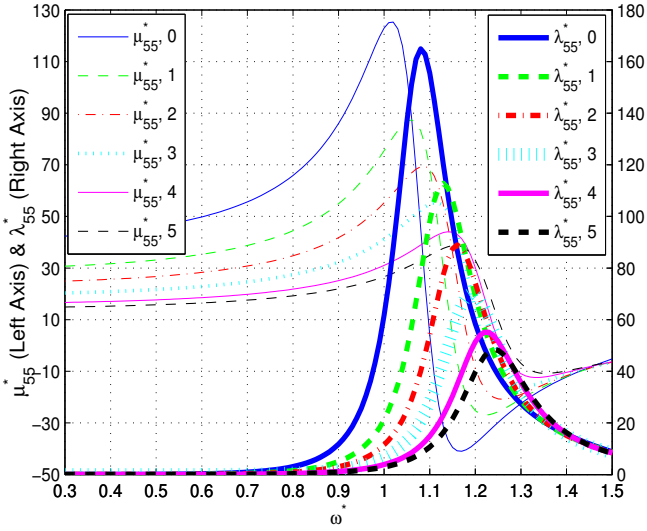

(e) Pitch-wave damping λ_{55} and added moment of inertia μ_{55}

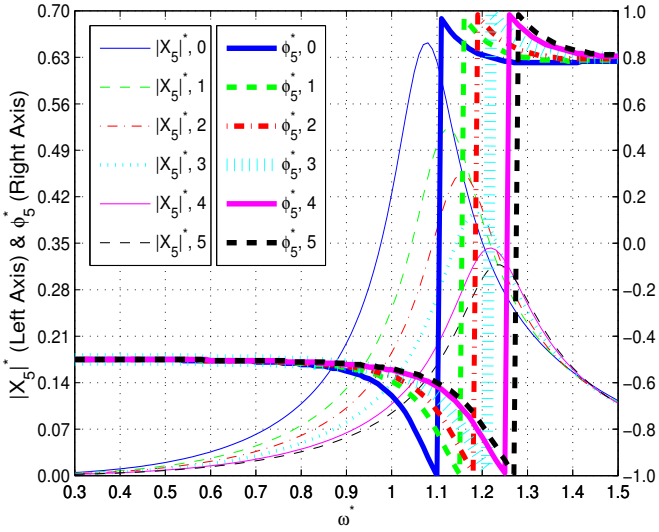

(f) Pitch-wave exciting torque magnitude $|X_5|$ and phase ϕ_5

Fig. 4. The nondimensional surge, heave, and pitch hydrodynamic radiation and wave excitation coefficients versus number of open flaps for a submergence depth of 1.4 m and plate length of 20 m. The nondimensional values are given by: $\mu^*_{11} = \mu_{11}/m$, $\lambda^*_{11} = \lambda_{11}/\omega m$, $|X_1|^* = |X_1|/\rho g w t$, $\mu^*_{33} = \mu_{33}/m$, $\lambda^*_{33} = \lambda_{33}/\omega m$, $|X_3|^* = |X_3|/\rho g w l$, $\mu^*_{55} = \mu_{55}/I_{55}$, $\lambda^*_{55} = \lambda_{55}/\omega I_{55}$, $|X_5|^* = |X_5|/\rho g l^2 w$, $\phi^*_i = \phi_i/\pi$, $\omega^* = \omega\sqrt{h/g}$.

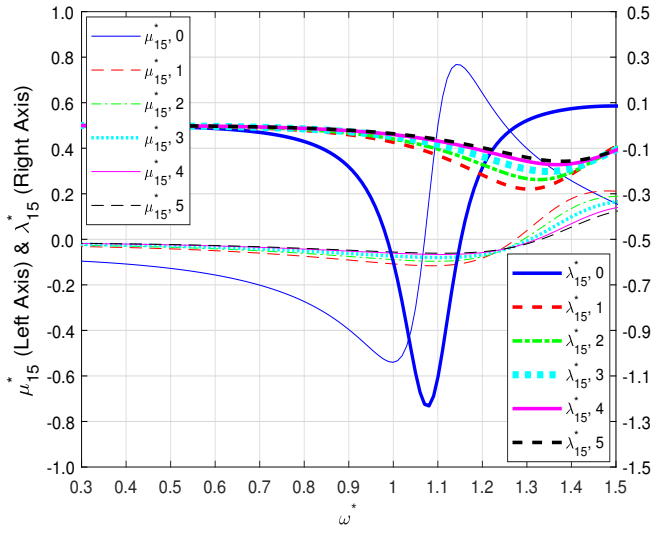

Fig. 5. The nondimensional surge-pitch hydrodynamic radiation coefficients versus number of open flaps for a submergence depth of 1.4 m and plate length of 20 m. The nondimensional values are given by: $\mu^*_{15} = \mu_{15}/\rho w^2 lt$, $\lambda^*_{15} = \lambda_{15}/\omega\rho w^2 lt$, and $\omega^* = \omega\sqrt{h/g}$.

to the phase difference between the heave and pitch motion of the plate; see Fig. 6d and 6e. Referring back to (24) and (25), the pitch motion of the plate will have opposite effects on the axial extension of PTO 1 and PTO 2. At the wave frequencies where PTO 1 produces negligible power, the heave and pitch motion of the plate are out of phase by approximately π rads, which results in the maximum heave motion occuring at the moment of minimum pitch rotation. For PTO 1, the contribution from the plate heave motion to the axial extension will then be offset by the axial compression that occurs because of the negative pitch rotation. In this situation, the axial extension of PTO 1 is minimized, almost motionless, while the axial extension of PTO 2 is amplified as a result of the positive phase coupling between the heave and pitch motion. For all wave frequencies, the 0 open flap configuration absorbs the greatest amount of power; however, over the frequency ranges of 0.6 to 0.7 and 1.1 to 1.2 there is little difference in the power produced by the other open flap configurations.

Fig. 4c plots the surge response amplitude operator where the peak in surge amplitude increases with each additional variable geometry flap opened. The first local peak in the surge response amplitude operator occurs near the pitch resonance frequency while a second peak occurs at more than 1.3 rad/s coinciding with the surge resonance. However, as additional flaps are opened, the surge displacement will further exceed the response amplitude operator limit of 3 that maintains the small angle approximation; refer to (23). The small angle approximation will be valid for all flap configurations at low wave amplitudes, but will be affected by the nonlinear PTO dynamics with increasing wave amplitude. The PTO axial force follows a profile similar to the absorbed power with the 0 open flap configuration generating the largest forces; see Fig. 6f. The force generated by PTO 2 dominates PTO 1 except in the low frequency range, where the two are nearly equal. In this range, the PTO axial extension is solely due to heave motion, and equivalent forces are generated in the PTO units. There is also a local minimum in the axial force of PTO 2 around the pitch resonance frequency; however, the drop is minimal compared to the reduction in the axial force of PTO 1.

VI. Conclusion

This paper has investigated a novel WEC device concept that has combined a submerged pressure differential plate with variable geometry modules. The two variable geometry modules consisted of five identical flaps that act as control surfaces. The variable geometry flaps were allowed to rotate around their central axis but were controlled in a binary fashion allowing for fully closed, $\varphi = 0$ deg, or fully open, $\varphi = 90$ deg configurations. If the variable geometry flaps were allowed to operate at intermediate angles, perhaps larger and fewer flaps could used as greater control over the hydrodynamics are afforded; however, based on the authors' previous research [2] there can be large changes in the hydrodynamics when adjusting the angle of rotation by small increments, which may be difficult to accurately model given uncertainties in measurements from rotary sensors. Therefore, additional research is required to understand the dynamic effects of controlling one or more variable geometry flaps on a wave-to-wave timescale.

Controlling the variable geometry modules quasi-statically was shown to be effective at altering the device geometry to reduce wave and PTO loading. The authors expect that improved control of the operational design loads, provided by the variable geometry modules, can improve the capacity factor of the device in larger sea states. Furthermore, the variable geometry design was shown to be capable of tuning the radiation coefficients to control the power output of each PTO and shift the wave frequency that maximizes the surge, heave, and pitch response of the absorber body. The current analysis has investigated device performance in regular waves, while assuming the PTOs are modeled using identical spring and damping coefficient; however, we expect that the power output could be further optimized using separate damping coefficients or using a more advanced control strategy.

The device performance was evaluated using linear hydrodynamic theory in the frequency domain. This linearization of the PTO dynamics is required to couple the fore and aft PTOs to the motion of the absorber body. In the linearization process, limits were derived for the absorber body motion that would have allowed the linear response to remain valid; however, there were wave frequency and flap configuration combinations that may exceed these limits in larger waves. An immediate improvement would be to angle the mooring tether lines, rather than place them in a vertical orientation, as the surge motion is minimally controlled by the PTOs. Future work remains to evaluate the structural and actuator

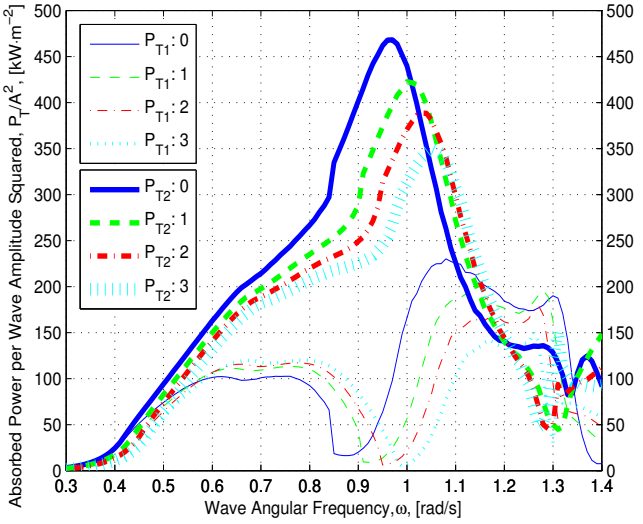

(a) Absorbed power per wave amplitude squared

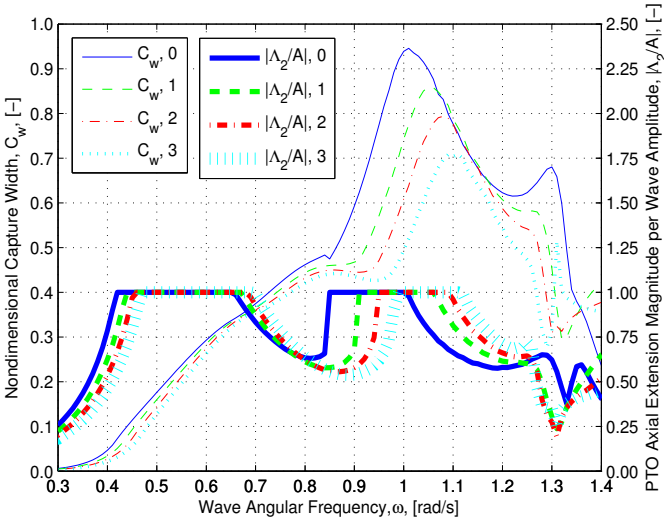

(b) Capture width and PTO 2 axial displacement

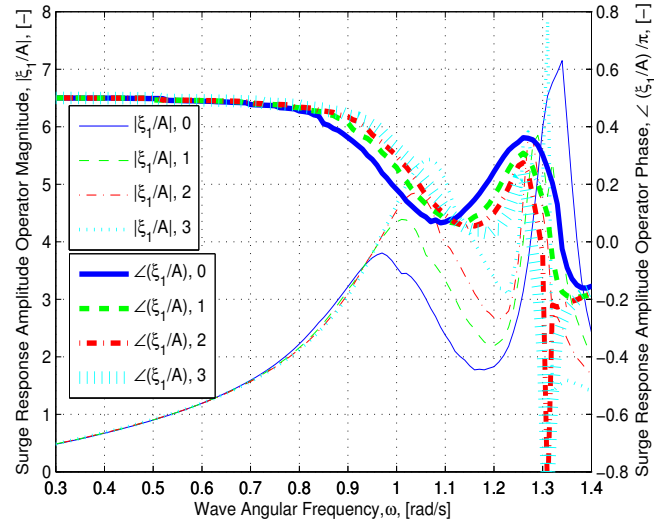

(c) Surge response amplitude operator magnitude and phase

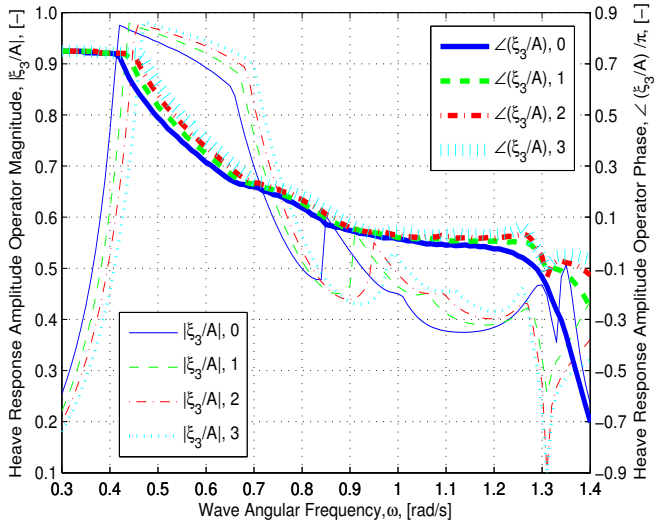

(d) Heave response amplitude operator magnitude and phase

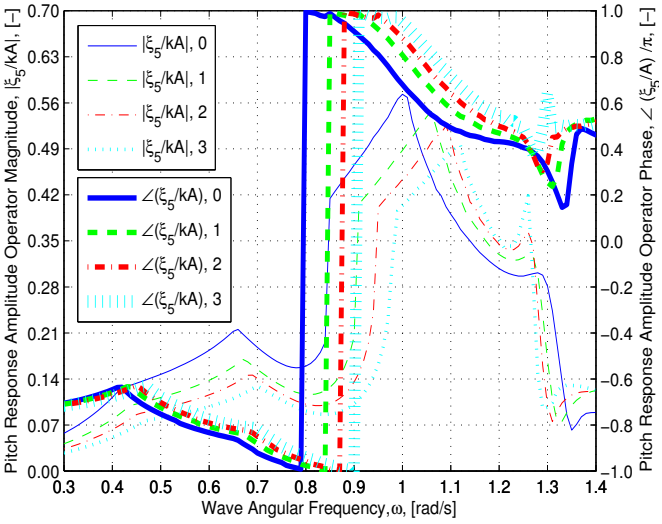

(e) Pitch response amplitude operator magnitude and phase

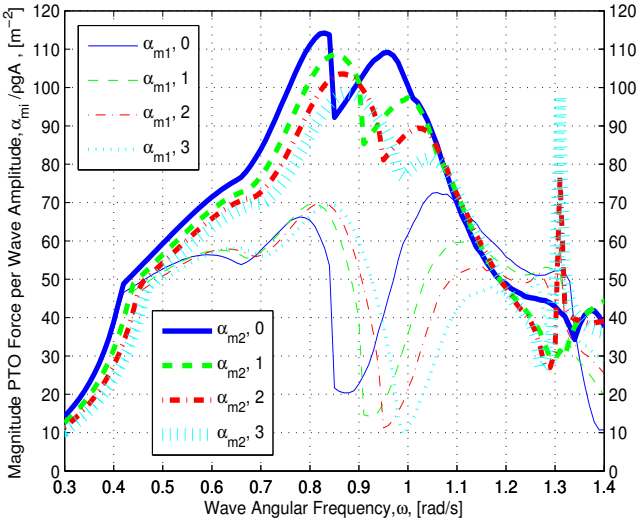

(f) Magnitude power take-off force per wave amplitude

Fig. 6. Absorbed power take-off power, nondimensional capture width, PTO axial force, and three degrees of plate motion versus number of open flaps. The results are presented for a plate length of 20 m, submergence depth of 1.4 m, and a spring extension length of 1 m. The numbers in the legend correspond to the number of open flaps.

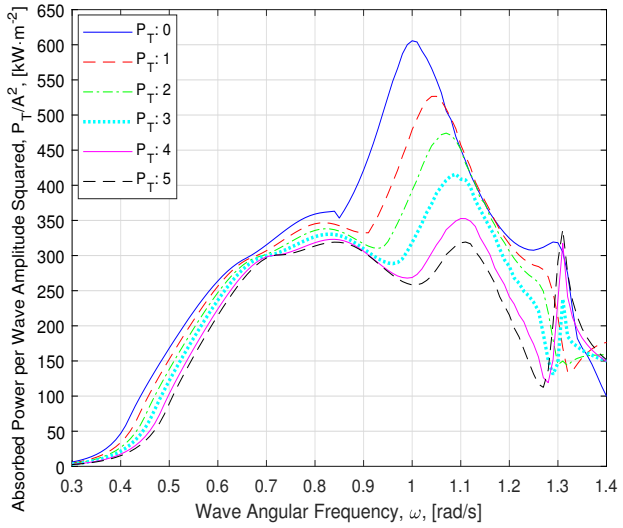

(a) Total absorbed power per wave amplitude squared

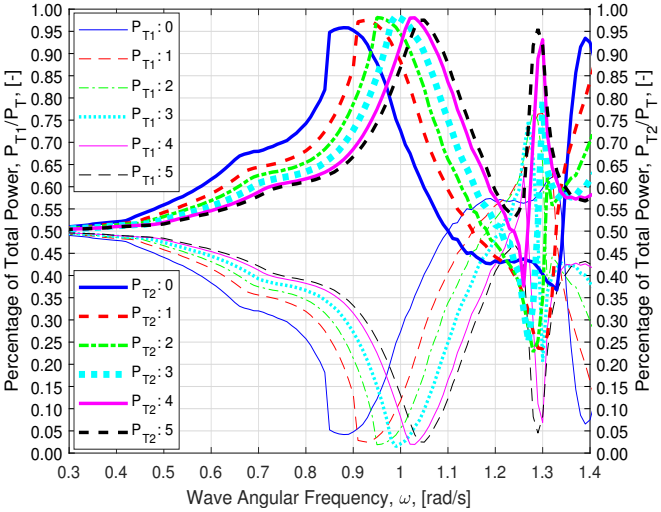

(b) Percentage of total absorbed power for each power take-off

Fig. 7. The total absorbed power and percentage of total absorbed power per power take-off versus the number of open flaps. The results are presented for a plate length of 20 m, submergence depth of 1.4 m, and a spring extension length of 1 m. The numbers in the legend correspond to the number of open flaps.

requirements to determine if the variable geometry design can be effectively controlled without adding significant capital and operational costs that would lead to a minimal reduction in the cost of energy.

REFERENCES

[1] T. Whittaker and M. Folley, "Nearshore oscillating wave surge converters and the development of Oyster," *Philos. T. Roy. Soc. A.*, vol. 370, pp. 345–364, 2012.

[2] N. Tom, M. J. Lawson, Y.-H. Yu, and A. D. Wright, "Preliminary analysis of an oscillating surge wave energy converter with controlled geometry," in *Eleventh European Wave and Tidal Energy Conference*, Nantes, France, 2015.

[3] N. Tom, Y.-H. Yu, and A. D. Wright, "Balancing the power-to-load ratio for a novel variable geometry wave energy converter with nonideal power take-off," in *Twelfth European Wave and Tidal Energy Conference*, Cork, Ireland, 2017.

[4] J. W. Weber and D. L. Laird, "Structured innovation of high performance wave energy converter technology," in *Eleventh European Wave and Tidal Energy Conference*, Nantes, France, 2015.

[5] A. Pecher, J. P. Kofoed, T. Larsen, and T. Marchalot, "Experimental study of the WEPTOS wave energy converter," in *31st International Conference on Ocean, Offshore, and Arctic Engineering*, Rio de Janeiro, Brazil, 2012.

[6] J. Chapman, A. Brask, J.-B. LeDreff, G. Foster, and G. Stockman, "Improving energy capture by varying the geometry of a novel wave energy converter," in *Twelfth European Wave and Tidal Energy Conference*, Cork, Ireland, 2017.

[7] M. Kelly, N. Tom, Y.-H. Yu, and R. Thresher, "Development of the second-generation oscillating surge wave energy converter with variable geometry," in *27th International Ocean and Polar Engineering Conference*, San Francisco, CA, USA, 2017.

[8] N. Tom, M. J. Lawson, Y.-H. Yu, and A. D. Wright, "Spectral modeling of an oscillating surge wave energy converter with control surfaces," *Appl. Ocean Res.*, vol. 56, pp. 143–156, 2016.

[9] M. A. Choiniere, N. M. Tom, and K. P. Thiagarajan, "Load-shedding characteristics of an oscillating surge wave energy converter with variable geometry," *Ocean Eng.*, under review.

[10] A. S. Zurkinden, S. H. Lambertsen, L. Damkilde, Z. Gao, and T. Moan, "Fatigue analysis of a wave energy converter taking into account different control strategies," in *32nd International Conference on Ocean, Offshore, and Arctic Engineering*, Nantes, France, 2013.

[11] N. Tom, Y.-H. Yu, A. D. Wright, and M. J. Lawson, "Balancing power absorption against structural loads with viscous drag and power take-off efficiency considerations," *IEEE J. Oceanic Eng.*, vol. 43 no. 4, pp. 1048–1067, 2018.

[12] R. P. F. Gomes, M. F. P. Lopes, J. C. C. Henriques, L. M.C. Gato, and A. F. O. Falcão, "The dynamics and power extraction of bottom-hinged plate wave energy converters in regular and irregular waves," *Ocean Eng.*, vol. 96, pp. 86–99, 2015.

[13] D. V. Evans, D. C. Jeffrey, S. H. Salter, and J. R. M. Taylor, "Submerged cylinder wave energy device: theory and experiment," *Appl. Ocean Res.*, vol. 1 no. 1, pp. 3–12, 1979.

[14] S. Crowley, R. Porter, and D. V. Evans, "A submerged cylinder wave energy converter," *J. Fluid Mech.*, vol. 716, pp. 566–596, 2013.

[15] M. Lehmann, R. Elandt, H. Pham, R. Ghorbani, M. Shakeri, M.-R. Alam, "An artificial seabed carpet for multidirecitonal and broadband wave energy extraction: Theory and experiment," in *Tenth European Wave and Tidal Energy Conference*, Aalborg, Denmark, 2013.

[16] F. Driscoll, J. Weber, S. Jenne, R. Thresher, L. J. Fingersh, D. Bull, A. Dallman, B. Gunawan, K. Ruehl, D. Newborn, M. Quintero, A. LaBonte, D. Karwat, and S. Beatty, "Methodology to calculate the ACE and HPQ metrics used in the Wave Energy Prize," Golden, CO: National Reneable Energy Laboratory. NREL/TP-5000-70592, pp. 1–47, 2018. [Online] Available: https://www.nrel.gov/docs/fy18osti/70592.pdf.

[17] M. A. Srokosz, "The submerged sphere as an absorber of wave power," *J. Fluid Mech.*, vol. 95 no. 4, pp. 717–741, 1979.

[18] A. Rafiee and A. Valizadeh, "Improving the hydrodynamic efficiency of point absorbers through coupling modes of motions," in *Twelfth European Wave and Tidal Energy Conference*, Cork, Ireland, 2017.

[19] A. Babarit, "A database of capture width ratio of wave energy converters," *Renew. Energy*, vol. 80, pp. 1015–1024, 2015.

[20] WAMIT Version 7.2 User Manual, http://www.wamit.com, 2016.

[21] D. V. Evans, "Maximum wave-power absorption under motion constraints," *Appl. Ocean Res.*, vol. 3, no. 4, pp. 200–203, 1981.

[22] P. McIver and D. V. Evans, "The occurance of negative added mass in free-surface problems involving submerged oscillating bodies," *J. Eng. Math.*, vol. 18, pp. 7–22, 1984.

[23] O. Faltinsen, Sea Loads on Ships and Offshore Structures. Volume 1 of Cambridge Ocean Technology Series. Cambridge: Cambridge University Press, 1993, pp. 47–49.

[24] J. N. Newman, Marine hydrodynamics. Massachusetts Institute of Technology Press, 1977, p. 296.